

The adsorption of dibenzothiophene using activated carbon loaded with cerium

Lin Xiong · Feng-Xiang Chen · Xue-Min Yan · Ping Mei

Published online: 28 September 2011
© Springer Science+Business Media, LLC 2011

Abstract Cerium-loaded activated carbon was prepared by classical soaking impregnation method and tested for dibenzothiophene adsorption from model fuels. The new adsorbents showed much better adsorption capacity and selectivity towards DBT than the virgin carbon. The adsorbents were characterized by N_2 adsorption, Boehm titration and FTIR. The improved performance is mainly due to changes in surface chemistry. The results show that the performance of activated carbon as desulfurization adsorbents can be considerably enhanced by a simple cerium loading method.

Keywords Adsorptive desulfurization · Activated carbon · Cerium · Dibenzothiophene

1 Introduction

Worldwide, much attention has been paid to deep desulfurization of transportation fuels due to the increasingly stringent regulations of the sulfur content specifications in these sulfur-containing fuels. Dibenzothiophene (DBT) and its derivatives are the refractory sulfur compounds in diesel, which are very difficult to be removed by the conventional hydrodesulphurization (HDS) processes [1]. Meanwhile adsorptive desulfurization provides an alternative technology of particular interest due to its low-energy consumption, the availability of regeneration of spent adsorbent and the ambient operation temperature and pressure [2]. Therefore extensive efforts have been made to find

adsorbent materials with both high capacity and good selectivity. Activated carbons with well-developed porous structure and unique surface properties have exhibited good potential as adsorbents for sulfur compounds and their adsorption capacity can be further improved by modification. It has been shown that introducing certain active species to the surface of activated carbons is an effective method to enhance the (DBT) removal capacity. So far activated carbons modified by various active species such as sulfur [3], silver [4], cobalt [5], sodium, copper [6] zinc, iron [7] zirconium [8] and nickel [9] have been investigated.

Although cerium loaded zeolites have been reported to show good [10–12] sulfur removal performance, and the S–M interaction mechanism between Ce^{4+} and sulfur atom in organic sulfur compounds has been proposed by Song et al. [13, 14], reports concerning cerium-loaded carbon-based adsorbents are still seldom. In this study cerium-loaded activated carbons were prepared and tested as adsorbents for DBT. A classical soaking impregnation method was adopted, but the impregnated carbons were calcined in air rather than inert atmosphere as impregnation modifications usually does. This is because thermal oxidation has been reported to benefit the adsorption capacity of activated carbon by introducing new surface acidic oxygen-containing groups [15]. In this study it was expected the oxidation and loading modification could have a synergetic effect on enhancing the adsorption capacity and selectivity of the primary carbon.

2 Experimental

2.1 Adsorbents preparation

For the preparation of cerium-loaded activated carbon, a soaking impregnation process was used. A commercially

L. Xiong · F.-X. Chen · X.-M. Yan (✉) · P. Mei
College of Chemistry and Environmental Engineering, Yangtze University, Jingzhou 434023, China
e-mail: yanzhangmm2002@163.com

available activated carbon (coconut shell based, Nantong, China) was used as the carbon support. The as-received activated carbon was washed with boiling deionized water and dried at 373 K overnight before impregnation. The washed carbon was denoted as AC. Then 5 g AC was added to 100 mL $(\text{NH}_4)_2\text{Ce}(\text{NO}_3)_6$ aqueous solution of a certain concentration (0.0025–0.015 M). The mixture was stirred for 24 h at room temperature. Then the excess solvent was slowly removed by evaporating at 50 °C and the residue was dried at 373 K overnight. Finally the sample was placed in a crucible and calcined at 350 °C for 4 h within a muffle furnace to decompose the precursor. The theoretic cerium loading of each sample was calculated from the concentration of $(\text{NH}_4)_2\text{Ce}(\text{NO}_3)_6$ aqueous solution, and the sample loaded with x mmol cerium per gram carbon was labeled as Ce/AC(x). For comparison the AC without impregnation was also calcined at 350 °C for 4 h and designated as ACO. All the samples prepared were kept in a desiccator until use.

2.2 Adsorption experiments

To evaluate the adsorption capacity of the adsorbents, adsorptive desulfurization of a model fuel was performed in batch mode at a constant temperature of 30 °C. The model fuel with sulfur content of 500 ppmw was obtained by dissolving DBT (Sigma-Aldrich) dissolved in petroleum ether (Fuchen Chemical Reagent company, Tianjin, China) and was designated as MF1. The kinetic studies were firstly performed to determine the equilibration time of the system. For a typical following adsorption test, a certain amount of adsorbent was added to a bottle containing 20 mL MF1. The covered bottle was then placed in a water bath and kept at 30 °C for 24 h. After equilibrium the concentration of DBT in the solution was determined using a UV spectrophotometer (SHIMADZU, UV-2450) at the corresponding wavelength. The adsorption capacity was expressed by the amount of sulfur adsorbed per unit mass of adsorbent and was calculated from the formula

$$q_e = V(C_0 - C_e)/m \quad (1)$$

where q_e is the equilibrium amount adsorbed, V is the volume of the liquid phase, C_0 is the initial concentration of sulfur before exposed to adsorbent, C_e is the concentration of sulfur at equilibrium, and m is the mass of the adsorbent. The adsorption isotherms were obtained by using 0.25–1 g adsorbents for desulfurization of 20 mL MF1.

To evaluate the adsorption selectivity of the adsorbents, a series of model fuels with sulfur content of 500 ppmw and benzene content of 10–40 wt% was firstly prepared using petroleum ether as the solvent. Then the adsorbents were used in desulfurization of these model fuels in the

same procedure as described above. The sulfur contents in the model oils after adsorption were analyzed using gas chromatography with flame ionization detector (GC–FID).

2.3 Regeneration of spent adsorbents

To test the reusability of adsorbents, 0.5 g spent adsorbents which was saturated after desulfurization of 20 mL MF1 was washed with toluene for 3 times. Each time the adsorbent was mixed with 20 mL toluene and kept at 80 °C for 2 h. The washed adsorbent was dried at 120 °C overnight to remove the remaining toluene. Then the recycled adsorbent was reused in desulfurization of 20 mL MF1 again. By this solvent-washing method, the adsorbents were reused for three times.

2.4 Characterization of adsorbents

Porous structure. The porous structures of the adsorbents were characterized by adsorption/desorption of nitrogen at -196 °C using a Micromeritics ASAP 2020 analyzer. Before the experiments, the samples were degassed for 6 h under vacuum at 120 °C. The specific surface area S_{BET} was calculated by the Brunauer-Emmett-Teller (BET) method. The total pore volume V_{total} was estimated by the liquid N_2 volume at relative pressure of 0.98. The micro-pore volume V_{micro} and micro-pore area S_{micro} were calculated using the t-plot method. The pore-size distribution was derived from the adsorption branches of the isotherms by using the Barrett–Joyner–Halenda (BJH) method.

Surface chemistry. The oxygenated surface groups were determined according to Boehm titration method [16], of which the details can be found elsewhere [17]. FT–IR spectra for samples were recorded using a Nicolet 6700 spectrometer with a resolution of 4.0 cm^{-1} using the attenuated total reflectance method (ATR). The spectrum was collected 16 times and corrected for the background noise. The experiments were done on the powdered samples, without KBr addition.

3 Results and discussion

Figure 1 shows the effect of adsorption time on adsorptive capacity of AC at 30 °C. The sulfur absorbed increased with time in the first 18 h. After that, the absorbed amount almost did not change, indicating the equilibrium was reached and the equilibrium adsorption capacity of AC was 7.02 mg-S/g-A (milligram of sulfur per gram of adsorbent). In the following adsorption tests, the adsorption times were all set to be 24 h.

Figure 2 shows the equilibrium adsorption capacity of AC with varying cerium loadings. All the samples loaded

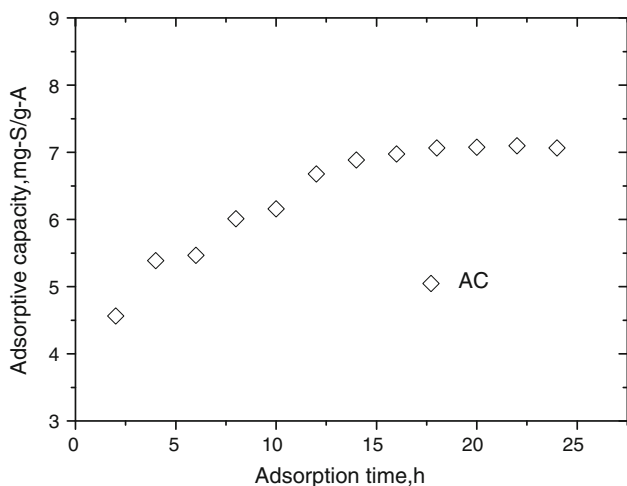


Fig. 1 Effect of adsorption time on the adsorptive capacity of AC at 30 °C, employing a model fuel/adsorbent ratio of 20 mL/0.75 g

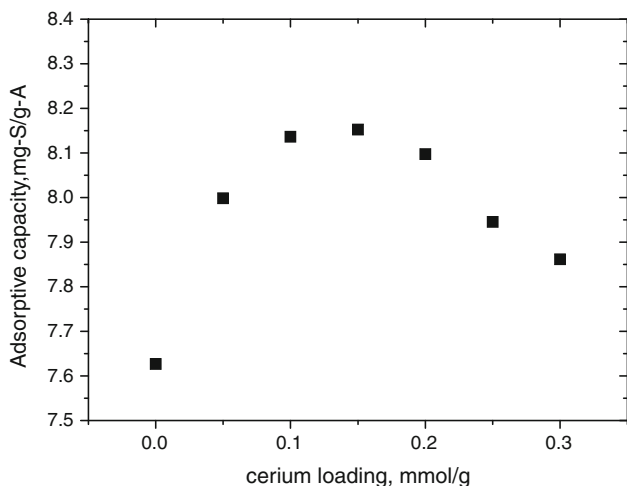


Fig. 2 Effect of cerium loading on the equilibrium adsorptive capacity at 30 °C, employing a model fuel/adsorbent ratio of 20 mL/0.75 g

with cerium showed higher capacity than the one without loading viz., ACO. The equilibrium adsorption capacity initially increased with cerium loading from 7.62 mg-S/g-A for ACO to 8.15 mg-S/g-A for Ce/AC(0.15). This indicates the loaded cerium introduced new adsorption sites to the original carbon. However, the equilibrium adsorption capacity decreased at even higher cerium loading and declined to 7.86 mg-S/g-A when cerium loading reached 0.3 mmol/g. This degeneration could be caused by reduced pore volume or pore blockage resulted from the high loading, which can be reasonably inferred from the subsequent pore characterization. It also should be noted the adsorption capacity of ACO was considerably higher than AC from Fig. 1. This is due to the oxidation effect caused by calcining at 350 °C.

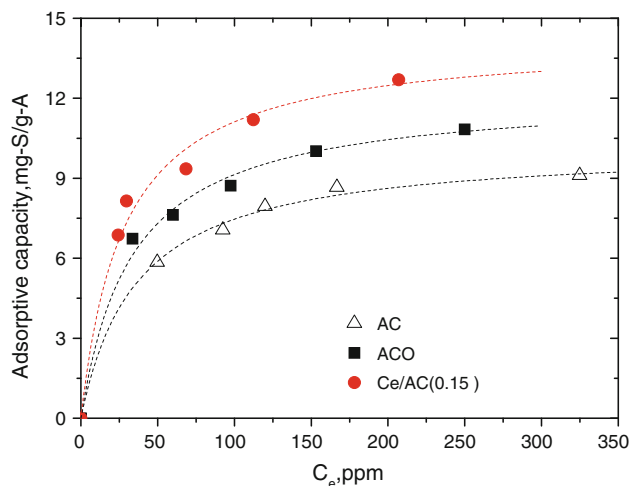


Fig. 3 Adsorption isotherms of AC, ACO and Ce/AC(0.15) at 30 °C. The dashed lines correspond to the fits of the Langmuir adsorption model to the equilibrium data

Figure 3 illustrates the DBT adsorption isotherms on AC, ACO and Ce/AC(0.15). All of them belong to the L type in the Giles classification [18], which indicates that as more sites in the substrate are filled, it becomes increasingly difficult for a fresh solute molecule to find a vacant site. This shape of isotherm is also characteristic of systems with no strong competition of the solvent for the active sites of adsorption. The adsorption isotherms show a tendency to reach a plateau at high equilibrium concentration of sulfur (i.e., low dose of adsorbent). The isotherms were fitted to Langmuir adsorption model in Fig. 4 according to the following relationship,

$$q_e = \frac{K \cdot q_m \cdot C_e}{1 + K \cdot C_e} \tag{2}$$

where C_e and q_e are the concentrations of total sulfur in the liquid phase and adsorbed phase at equilibrium, respectively. The adsorption equilibrium constant is K . The maximum adsorption capacity of total sulfur corresponding to the saturation coverage of the surface by sulfur compounds is represented by q_m . The excellent goodness of the fit (in all cases $R^2 > 0.99$) indicates that the Langmuir equation is suitable for application for the systems studied. The calculated q_m values are 10.2, 12.2 and 14.2 mg-S/g-A for AC, ACO and Ce/AC(0.15), respectively. This demonstrates that cerium loaded by this method greatly enhanced the adsorption capacity of carbon, although thermal oxidation may also contribute partially to the increase of adsorption capacity.

Figure 5 shows the effect of benzene on the adsorption capacity of AC, ACO and Ce/AC(0.15). For all samples the adsorption capacity declined considerably as the content of benzene in model fuel increased. This is due to the strong competitive adsorption of benzene onto carbon surface [19].

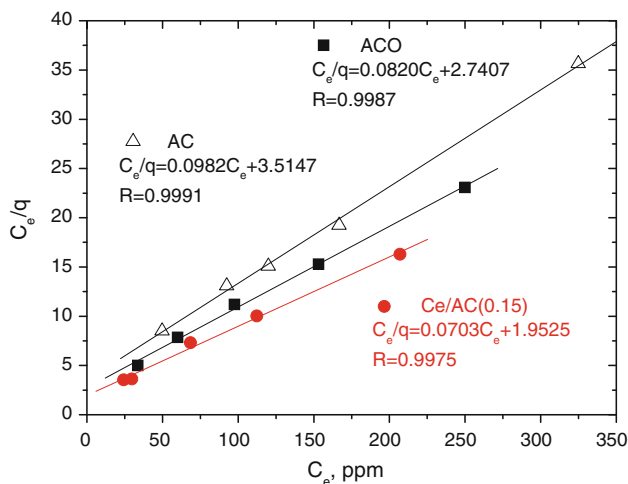


Fig. 4 Plots of C_e/q versus C_e for AC, ACO and Ce/AC(0.15)

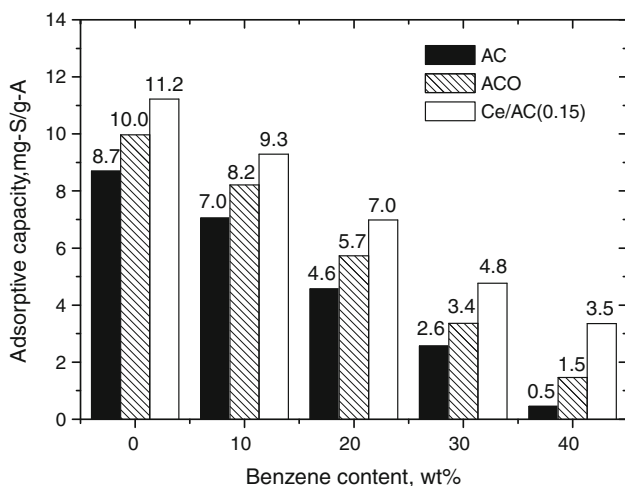


Fig. 5 Effect of benzene content in the model fuel on the adsorptive capacity at 30 °C, employing a model fuel/adsorbent ratio of 20 mL/0.5 g

However, it could be seen the adsorption capacity of Ce/AC(0.15) declined more slowly than that of AC and ACO. When the benzene content increased from 0 to 40%, the adsorption capacity of AC, ACO and Ce/AC(0.15) declined by nearly 95, 85 and 70%, respectively. Therefore the advantage of cerium loaded carbon becomes more significant as the benzene content becomes higher. It is well known that the selectivity is usually the consequence of specific chemical interaction rather than dispersive forces. In this case, the oxygen groups produced by heat treatment can lead to improved selectivity through acid–base interaction with DBT [3, 20, 21]. However, the much better selectivity of Ce/AC(0.15) than ACO suggests the cerium also played an important role in selective adsorption.

Figure 6 shows the reusing ability of AC and Ce/AC(0.15). It can be seen that for both adsorbents, the

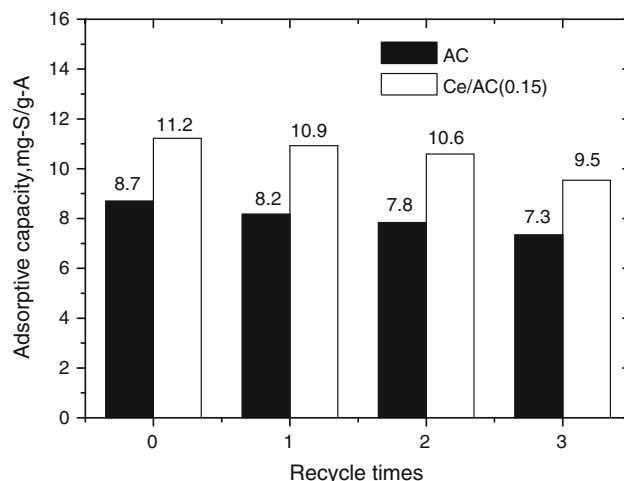


Fig. 6 The reusing ability of AC and Ce/AC(0.15) at 30 °C, employing a model fuel/adsorbent ratio of 20 mL/0.5 g

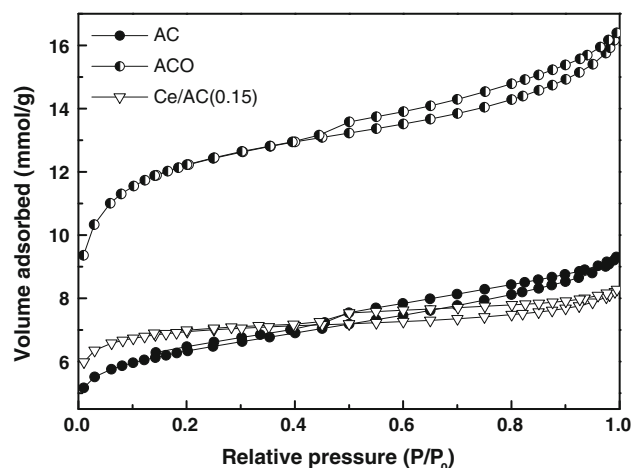


Fig. 7 Nitrogen adsorption/desorption isotherms for AC, ACO and Ce/AC(0.15) at -196 °C

adsorption capacity decreased slightly after every recycle due to retained sulfur compound after washing. After three times regeneration, the adsorption capacity of Ce/AC(0.15) is still higher than that of AC. The stable reusing ability of Ce/AC(0.15) suggests there is no significant cerium loss during the adsorption and solvent-washing process.

Nitrogen adsorption–desorption isotherms of AC, ACO and Ce/AC(0.15) are shown in Fig. 7. All the samples show major nitrogen uptake at relative pressures less than 0.25. This indicates the samples are highly microporous. A small hysteresis loop can also be observed at high relative pressures for three samples indicating the presence of mesopores. The slope of the isotherms increases in the order: Ce/AC(0.15) < AC < ACO, implying increasing textural heterogeneity and broader pore size distribution. The above analysis can be more clearly observed from Fig. 8.

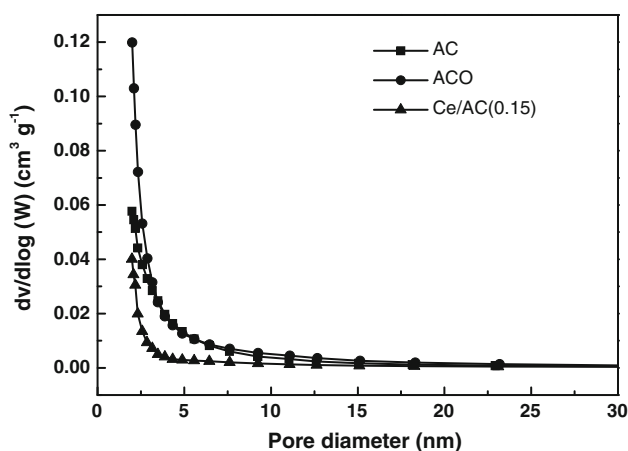


Fig. 8 Pore-size distributions of AC, ACO and Ce/AC(0.15)

Table 1 Textural properties evaluated from N₂ adsorption

Adsorbents	S _{BET} (m ² g ⁻¹)	V _{total} (cm ³ g ⁻¹)	Average pore size (nm)	V _{micro} (cm ³ g ⁻¹)	S _{micro} (m ² g ⁻¹)
AC	484	0.31	2.58	0.14	301
ACO	936	0.55	2.33	0.28	604
Ce/ AC(0.15)	525	0.28	2.12	0.19	425

The estimated texture parameters on the basis of the nitrogen adsorption–desorption isotherms are summarized in Table 1. After calcining ACO shows greatly increased total porosity and surface area than AC. This may be due to the gasification of carbon during the calcining, which may cause pore-widening or formation of new pores. On the other hand, the textural change for Ce/AC(0.15) is relatively small. This could be explained by the pore volume occupied by loaded cerium species. Among these textural parameters, special emphasis should be paid to micro-pore volume, which has been recognized to have the highest affinity for physical adsorption via dispersive forces [17, 22]. The micro-pore volume of the samples increases in the order: AC < Ce/AC(0.15) < ACO. This suggests factors other than micro-pore volume should be involved to account for the higher adsorption capacity of Ce/AC(0.15) than ACO.

Table 2 shows the number of surface groups of AC, ACO and Ce/AC(0.15) evaluated from Boehm titration. It can be seen that ACO has more acidic surface groups than

Table 2 Number of surface groups evaluated from Boehm titration

Adsorbents	Carboxylic (mmol/g)	Lactonic (mmol/g)	Phenolic (mmol/g)	Total acidic (mmol/g)	Total basic (mmol/g)
AC	0.048	0.087	0.023	0.158	0.793
ACO	0.064	0.091	0.107	0.262	0.769
Ce/AC(0.15)	0.066	0.110	0.112	0.288	0.768

AC due to heat treatment, and Ce/AC(0.15) shows even higher amount of acidic surface groups than ACO. The cerium salt impregnation could lead to additional oxidation of carbon surface in two ways: firstly, the redox of Ce⁴⁺/Ce³⁺ facilitates the adsorption of oxygen on carbon surface and thus promotes carbon oxidation reaction [23, 24]; secondly, the reduction of nitrate during precursor decomposition could also lead to oxidation of carbon [25].

Based on the N₂ adsorption and Boehm titration results, the best adsorption capacity of Ce/AC(0.15) among the three samples should be mainly attributed to the changes in surface chemistry. The cerium impregnation may have twofold benefits for the adsorption of DBT on activated carbon: increasing the oxidation degree of the carbon surface as well as providing new active metal sites. The high-valence cerium ion could either form S-M bond with DBT [13] or promote oxidation of DBT like some other metal species such as silver [5], copper and iron [26]. These reactive adsorption mechanisms also account for the high adsorption selectivity of Ce/AC(0.15).

Figure 9 shows the FTIR spectra of AC and the modified carbons. Almost no peaks could be identified for AC, and the changes for the modified carbons are also not prominent except for some very weak peaks. This is a consequence of the strong IR adsorption of activated carbon and therefore a reference spectrum is usually used to manifest the changes of surface groups after modification [27].

Figure 10 shows subtraction FTIR spectra based on AC spectrum for the modified carbons. From this figure it can be clearly seen that ACO shows two adsorption bands around 1,150 and 1,580 cm⁻¹, which could be assigned to C–O stretching and aromatic C = C stretching enhanced by adsorbed oxygen., respectively. These two bands have also been observed by others on high temperature O₂ treated carbons [28]. For Ce/AC(0.05), the IR spectrum do not show much difference to ACO except the increase in intensity of the two bands around 1,150 and 1,580 cm⁻¹ and a small peak at 1,720 cm⁻¹ which could be attributed to carbonyl stretch in the carboxylic acid groups [28]. When cerium loading reaches 0.1 mmol/g or higher, several new peaks at 1,080, 1,240 and 1,390 cm⁻¹ becomes identifiable while the band around 1,580 cm⁻¹ remains. The adsorption band around 1,080 cm⁻¹ has been reported to correspond to the Ce–O–C structure [29]. The other two bands with peaks at 1,240 and 1,390 cm⁻¹ could be

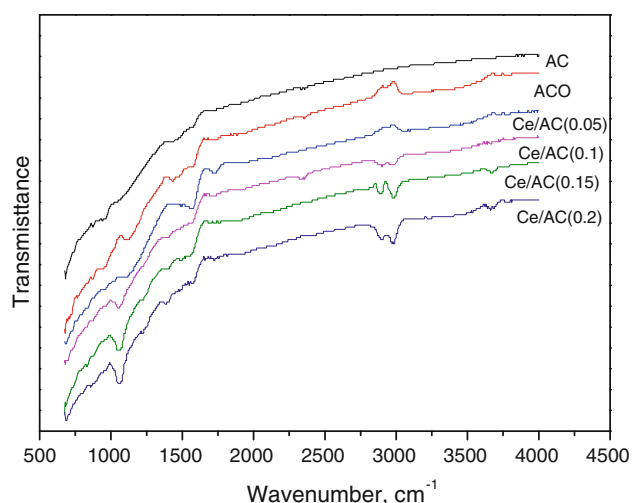


Fig. 9 FTIR spectra of AC and the modified carbons

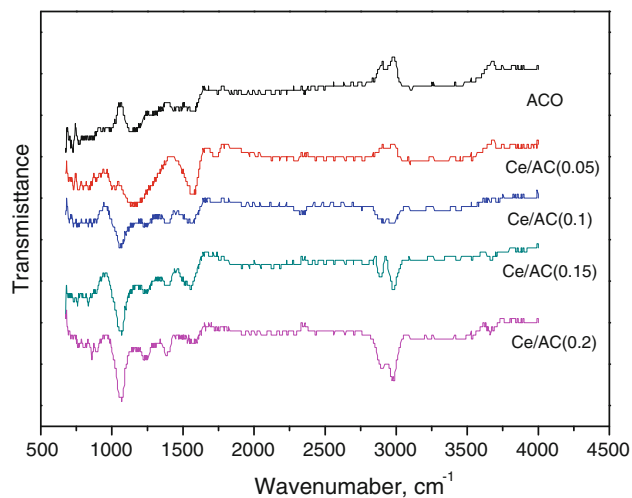


Fig. 10 Subtraction FTIR spectra based on AC spectrum for the modified carbons

assigned to C–O in ethers and carboxyl-carbonate structures [27], respectively. It is also interesting to find that as cerium loading increases, the adsorption band between 2,800 and 3,050 cm^{-1} associated with C–H stretching becomes stronger. Although the formation mechanism of this band needs further investigation, it is possibly related to the reaction of carbon during decomposition of $(\text{NH}_4)_2\text{Ce}(\text{NO}_3)_6$. The FTIR results demonstrate the modified carbons have more surface oxygen groups than the original carbon, which agrees well with the results obtained by Boehm titration.

4 Conclusion

Activated carbon loaded with cerium prepared by a soaking and calcining method shows greatly enhanced adsorption

capacity and selectivity towards dibenzothiophene. The loading modification does not change the textural properties of the original carbon very much. The improved performance is mainly due to the changes in surface chemistry of the adsorbent, in which the increased acidic sites and cerium ion may play important roles. The optimal cerium loading is determined to be 0.15 mmol/g for the carbon used. The Langmuir adsorption model fits the adsorption data for dibenzothiophene onto activated carbon-based adsorbents. The impregnated activated carbon also showed good recycling ability by toluene washing. The results show that the performance of activated carbon as desulfurization adsorbents can be considerably enhanced by a simple cerium loading method.

Acknowledgments Financial support from National Natural Science Foundation of China (No. 21106008) is gratefully acknowledged.

References

1. C. Song, X. Ma, *Appl. Catal. B Environ.* **41**, 207–238 (2003)
2. R.T. Yang, A.J. Hernandez-Maldonado, F.H. Yang, *Science* **301**, 79–81 (2003)
3. M. Seredych, T.J. Bandosz, *Carbon* **49**, 1216–1224 (2011)
4. B.C. Cao, W.Z. Shen, Y.H. Liu, *Adsorpt. Sci. Technol.* **26**, 225–231 (2008)
5. M. Seredych, T.J. Bandosz, *Energy Fuels* **23**, 3737–3744 (2009)
6. C.O. Ania, T.J. Bandosz, *Carbon* **44**, 2404–2412 (2006)
7. M.X. Yu, Z. Li, Q.B. Xia, H.X. Xi, S.W. Wang, *Chem. Eng. J.* **132**, 233–239 (2007)
8. L. Xiong, X.M. Yan, P. Mei, *Adsorpt. Sci. Technol.* **28**, 341–350 (2010)
9. G.X. Yu, J.B. Li, X.L. Zhou, C.L. Li, L.F. Chen, J.A. Wang, *Adv. Mater. Res.* **132**, 141–148 (2010)
10. F.P. Tian, W.C. Wu, Z.X. Jiang, Y.X. Yang, T.X. Cai, C. Li, *Chin. J. Cat.* **26**, 734–736 (2005)
11. M. Xue, R. Chitrakar, K. Sakane, T. Hirotsu, K. Ooi, Y. Yoshimura, M. Toba, Q. Feng, *J. Colloid Interface Sci.* **298**, 535–542 (2006)
12. J. Wang, F. Xu, W.J. Xie, Z.J. Mei, Q.Z. Zhang, J. Cai, W.M. Cai, *J. Hazardous Mater.* **163**, 538–543 (2009)
13. S. Velu, X.L. Ma, C.S. Song, *Ind. Eng. Chem. Res.* **42**, 5293–5304 (2003)
14. X.L. Ma, L. Sun, C.S. Song, *Catalysis Today* **77**, 107–116 (2002)
15. M.X. Yu, Z. Li, Q.N. Ji, S.W. Wang, D.G. Su, Y.S. Lin, *Chem. Eng. J.* **148**, 242–247 (2009)
16. H.P. Boehm, *Carbon* **32**, 759–769 (1994)
17. C.O. Ania, T.J. Bandosz, *Langmuir* **21**, 7752–7759 (2005)
18. C. Giles, T. Mc Ewan, S. Nakhwa, D.J. Smith, *J. Chem. Soc.* **4**, 3973 (1960)
19. C. Yu, J.S. Qiu, Y.F. Sun, X.H. Li, G. Chen, Z. Bin Zhao, *J. Porous Mater.* **15**, 151–157 (2008)
20. Y.X. Yang, H.Y. Lu, P.L. Ying, Z.X. Jiang, C. Li, *Carbon* **45**, 3042–3044 (2007)
21. J. Bu, G. Loh, C.G. Gwie, S. Dewiyanti, M. Tasrif, A. Borgna, *Chem. Eng. J.* **166**, 207–217 (2011)
22. M. Seredych, T.J. Bandosz, *Energy Fuels* **24**, 3352–3360 (2010)
23. L. Tian, C. Li, Q. Li, G. Zeng, Z. Gao, S. Li, X. Fan, *Fuel* **88**, 1687–1691 (2009)
24. S. Sumathi, S. Bhatia, K.T. Lee, A.R. Mohamed, *J. App. Sci.* **10**, 1052–1059 (2010)

25. J.C. Serrano-Ruiz, E.V. Ramos-Fernández, J. Silvestre-Albero, A. Sepúlveda-Escribano, F. Rodríguez-Reinoso, *Mater. Res. Bull.* **43**, 1850–1857 (2008)
26. M. Seredych, T.J. Bandosz, *Fuel Proc. Technol.* **91**, 693–701 (2010)
27. A. Dandekar, R.T.K. Baker, M.A. Vannice, *Carbon* **36**, 1821–1831 (1998)
28. P.E. Fanning, M.A. Vannice, *Carbon* **31**, 721–730 (1993)
29. B. Ksapabutr, E. Gulari, S. Wongkasemjit, *Mater. Chem. Phys.* **99**, 318–324 (2006)